Materials and Design 36 (2012) 663–670

Contents lists available at SciVerse ScienceDirect

Materials and Design

journal homepage: www.elsevier.com/locate/matdes

Investigation on the microstructure and mechanical properties of Ti–6Al–4V alloy joints with electron beam welding

Shaogang Wang *, Xinqiang Wu

College of Material Science and Technology, Nanjing University of Aeronautics and Astronautics, Nanjing 210016, China

ARTICLE INFO

Article history:
Received 28 September 2011
Accepted 30 November 2011
Available online 11 December 2011

Keywords:
A. Non-ferrous metals and alloys
D. Welding
F. Microstructure
Ti–6Al–4V alloy
Electron beam welding
Beam scanning pattern
Mechanical properties

ABSTRACT

Titanium and its alloys have excellent combination of properties, and they are extensively used in many industrial fields. However, due to their special weldability, the welding of titanium alloys is always of concern to many researchers. This work is aiming at investigation of the effect of different beam scanning patterns on the microstructure and mechanical properties of Ti–6Al–4V alloy joints by electron beam welding. The circular scanning pattern and linear scanning pattern are employed respectively during welding. Results show that the weld metal is full of cross–cross acicular α′ martensitic structure, while the base metal is of equiaxed structure. Mechanical property tests indicate that the hardness of weldment is higher than that of heat-affected zone (HAZ) and base metal. The tensile strength of joint is almost equal to that of base metal, and it is well in accordance with the relationship between microstructure and mechanical properties of welded joints. The tensile fracture morphology of joint presents obviously the characteristic of ductile fracture, which is related to the bigger and deeper dimples distributed on the surface of joint. The circular scanning pattern makes the joint microstructure coarse, while the linear scanning pattern meets the requirement of fining grains by uniform distribution of alloy elements or big grains being broken.

1. Introduction

Ti–6Al–4V alloy has excellent combination of properties such as low density, high specific strength and corrosion resistance, and it has been considered as one of preferential engineering materials extensively used in many industrial fields such as aerospace, shipbuilding, petrochemical and food industry [1–3]. Ti–6Al–4V alloy has two allotropic phases, namely, the body centered cubic (BCC) structured β phase and the hexagonal close-packed (HCP) structured α phase. The β phase distributes along the boundaries of α phase. It contains 6% aluminum for α stabilization and 4% vanadium for β stabilization, and when it is heated up to 882 °C, α phase transforms to β phase [4,5]. The final structure and properties of Ti–6Al–4V alloy and its weldment mainly depend on both the initial heat treatment state and cooling rate during welding [6,7]. Because titanium and its alloys have many special physicochemical and heat treatment features, great attention needs paying to their fabricating processes [8,9], particularly to welding.

Usually, it is a challenge to optimize welding parameters and obtain perfect welded joints [10]. The welding of Ti–6Al–4V alloy is difficult due to the fact that when the material is heated to the temperature over 250 °C, and especially at the molten stage, there exists a strong tendency of reaction with most atmospheric gases or elements such as hydrogen, oxygen, nitrogen or carbon [4,11]. These incidental elements will cause severe embrittlement of alloy, and reduce its ductility and toughness, while increasing its strength and hardness. Moreover, welded joints will be inferior in the case of improper preparation of the base material and filler metals before and during welding process, or impurities in the shielded gas, or improper shielding of weld zone, etc.

In the conventional welding process, Ti–6Al–4V alloy joints can be produced if contamination is carefully avoided [12]. While electron beam welding (EBW) is preferable to joining such alloys, since the vacuum shields molten pool from all incidental elements. What is more, with high energy density and relative low heat input, deep penetration joints can be achieved with just one bead [3,13,14]. At present, some investigations have been carried out on the microstructure and mechanical properties of titanium alloy welded joints [4,15]. Kishore Babu et al. [16] have investigated the effect of beam oscillation on fatigue life of Ti–6Al–4V electron beam weldments. However, there is hardly any literature reporting about the effect of beam scanning with different patterns on the microstructure and mechanical properties of titanium alloy joints. The previous work of authors demonstrated that the adding of electron beam scanning is advantageous to promote the fluidity of molten pool and diminish the porosity during welding, thus the quality of welded joint can be greatly improved [17]. Consequently, an

* Corresponding author. Tel.: +86 025 5211 2901; fax: +86 025 5211 2626.
E-mail address: sgwang@nuaa.edu.cn (S.G. Wang).

0261-3069/$ - see front matter © 2011 Elsevier Ltd. All rights reserved.
doi:10.1016/j.matdes.2011.11.068

attempt has been carried out to study the effect of different scanning patterns on microstructure and mechanical properties of welded joint. As a comparison, the welded joint without scanning is also produced.

2. Experimental materials and procedures

The base metal is Ti–6Al–4V titanium alloy in rolling state. The mechanical properties of base metal are shown in Table 1 and its microstructure is presented in Fig. 1. Fig. 1a is the image of optical microscope (OM), while Fig. 1b is the image of transmission electron microscopy (TEM). From Fig. 1, it can be seen that the base metal consists of duplex microstructure with primary equiaxed α phase and acicular β phase, which distributes in the interface of zonal α phase. Moreover, it indicates that the content of α phase is higher than that of β phase.

Before welding, the surface of titanium alloy plates are polished with emery paper and ablated in aqueous solution of 3%HF + 35%HNO_3. The titanium alloy plates with the dimension of 200 mm × 100 mm × 6 mm are welded in butt joint along the longitudinal direction. In order to get the penetration bead, the gap between two plates is necessary, which is 0.5–1 mm. Autogenous full-penetration electron beam weldments are produced with beam scanning technique (using circular waveform or linear waveform) and without beam scanning respectively. The patterns of circular and linear scanning are shown in Fig. 2 respectively ("*V*" indicates welding direction in Fig. 2). Attempts are carried out to determine the electron beam welding parameters in achieving a full penetration joint. The optimized welding parameters are listed in Table 2.

After welding, the microstructure and mechanical properties of joints with different welding parameters are investigated. The microstructures of the coupons are observed by MM6 optical microscopy. The phase constituent of weld metal is tested by D8 ADVANCE X-ray diffractometer (XRD). Besides, disk samples of 3 mm diameter with a hole in the center are applied to TEM observation and all samples are prepared by electropolishing in electrolyte of 6%$HClO_4$ + 34%C_4H_9OH + 60%CH_3OH under the temperature −20 to −30 °C. TEM observation is conducted by FEI Tecnai G2 TEM. The microhardness of weld metal, HAZ and base metal are tested by HXS-1000A microhardness Vicker with load 100 N and holding time 10 s. The tensile strength test is carried out by CMT 5105 electronic universal tester and the joint fracture is observed under Quanta 200 scanning electron microscopy (SEM).

3. Results and discussion

3.1. Microstructure

The microstructures of Ti–6Al–4V alloy weld metal with different parameters are shown in Fig. 3. There is no essential distinction among the four metallographs, and the martensitic phase transformation of all joints occurs to a certain degree. Without adding filler metal while welding, the weld metal comes only from the molten part of base metal. There are great differences in microstructure of weld metal which is carried out with the aid of a filler metal [18]. When the base metal is heated over β-transus temperature during welding, titanium alloy will melt rapidly and fill into the gap between two plates, subsequently, in the rapid cooling process, the martensite phase transformation from high temperature β phase takes place and α′ is formed with the basket weave.

As illustrated in Fig. 3a, microstructure with circular waveform scanning shows a relatively bigger crystal grains as against those without scanning or with linear scanning. In the weldment there are some colonies of acicular α′ phase obviously in a certain direction. Fig. 3b and c show that the α′ phase in weld metal of joints B2 and B3 is a little finer than in joint B1. Acicular α′ phase in joint B2 distributes along some directions, and the feature of reticular structure is not distinct, while α′ martensitic phase in joint B3 presents basket weave. Crystal nucleus of α′ phase comes into being along the boundaries of or in β phase at the same time, and large amounts of secondary α′ phase generate based on the previous α′ phase, while more α′ phase concentrates in the unit region. The microstructure of joint B4 weld metal without electron beam scanning is shown in Fig. 3d. The width of α′ phase is a little longer, and the distribution morphology marks between joints B2 and B3.

Different microstructure characterizations of joints show that transformation of microstructure occurred from an equiaxed to an acicular structure. This kind of distinction attributes to the maximum temperature, melting of base metal as well as subsequent cooling with different cooling rate [19]. The beam scanning may result in fining the grains, and the effect of linear scanning is much better than that of circular scanning, as will be discussed in more detail in the following text.

Table 1
Mechanical properties of Ti–6Al–4V alloy plate (20 °C).

Tensile strength σ_b (MPa)	Yield strength σ_s (MPa)	Microhardness (HV)	Elongation δ (%)	Section shrinkage ψ (%)
935	890	360	13	22

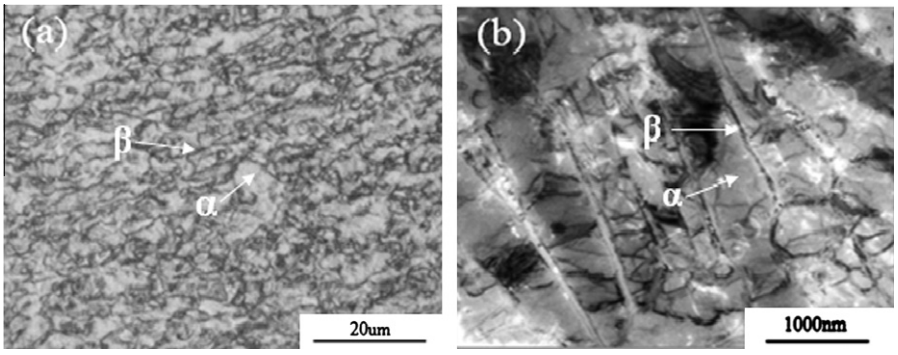

Fig. 1. Microstructure of Ti–6Al–4V alloy base metal: (a) OM image and (b) TEM image.

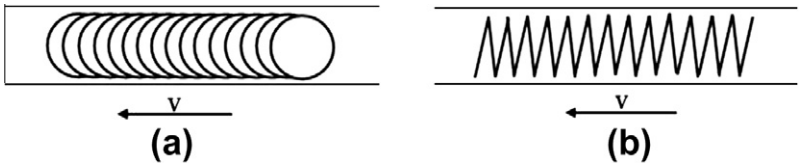

Fig. 2. The patterns of electron beam scanning: (a) circular scanning and (b) linear scanning.

Table 2
Electron beam welding parameters.

No.	Welding voltage U (kV)	Working distance L (mm)	Beam current I (mA)	Welding speed V (mm min^{-1})	Beam scanning		
					Scanning pattern	Amplitude VX/VY	Frequency f (Hz)
B1	60	200	50	900	Circle	3/3	800
B2	60	200	40	600	Line	3/3	800
B3	60	200	40	300	Line	3/3	–
B4	60	200	30	300	–	–	–

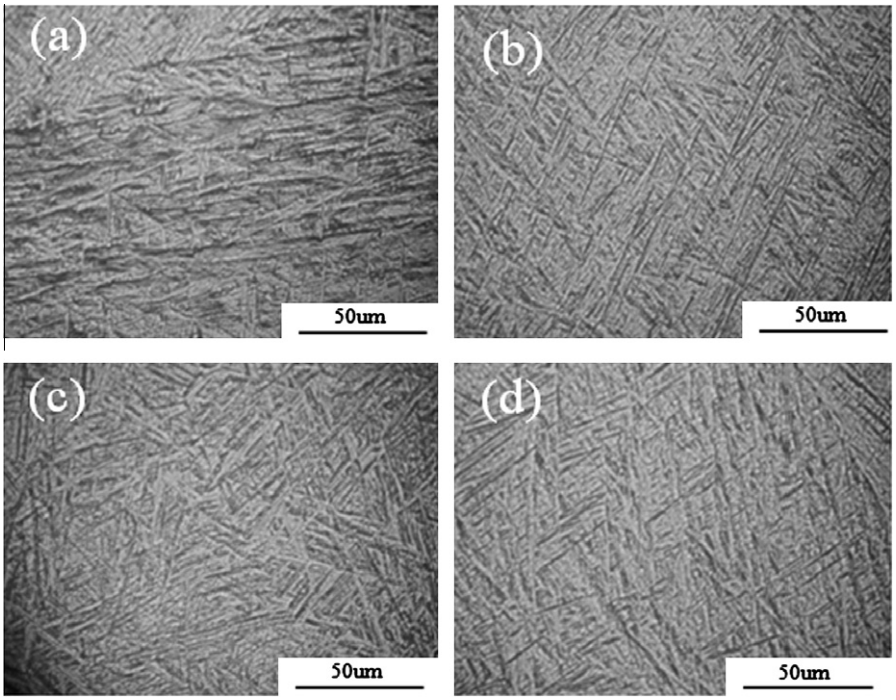

Fig. 3. Microstructures of Ti–6Al–4V EBW weld metal: (a) joint B1, (b) joint B2, (c) joint B3 and (d) joint B4.

In contrast, there are still some differences between the weldment of joints B1 and B3. In order to determine the phase constitution of weld metal, XRD patterns of joints are measured, as shown in Fig. 4. It indicates that the fusion zone (FZ) nearly consists of α′ martensitic phase but a small quantity of β phase. From the phase constitution, there does not exist obvious difference between the two joints, and there are not any other phases in their diffraction patterns. The nearly mono-phase martensitic structure contributes greatly to the mechanical properties of welded joints.

Further analysis of the microstructure of weldment B3 is carried out, and the TEM images are shown in Fig. 5. From the micrographs, it can be clearly seen that acicular α′ phase with different width staggeringly distributes in various layers. The acicular α′ phase presents different sizes, and some are narrow and long, while some are wide but short. In Fig. 5a and b, many parallel secondary acicular α′ come out from the coarse dendritic crystal. The molten materials have not generated lots of crystal nucleus at the same time, and parts of crystal nucleus come out simultaneously or ones after ones. The primary α′ phase produced has sufficient time to grow quickly and hinders the following ones, or becomes broken some time. The fragile dendritic crystals melts under latent heat during solidification, getting lots of nucleus and growing attached to the bigger grains that results in rapid growth, thus the single acicular α′ is formed, as shown in Fig. 5c. The complex microstructure could be formed in the weldment when the appropriate welding parameters with linear beam scanning are used.

During the welding of Ti–6Al–4V alloy, the phase transformation of weld metal is quite complex. In the heating process, original β phase transforms to high-temperature β phase promptly when rapid thermal shock comes from electron beam, and original α

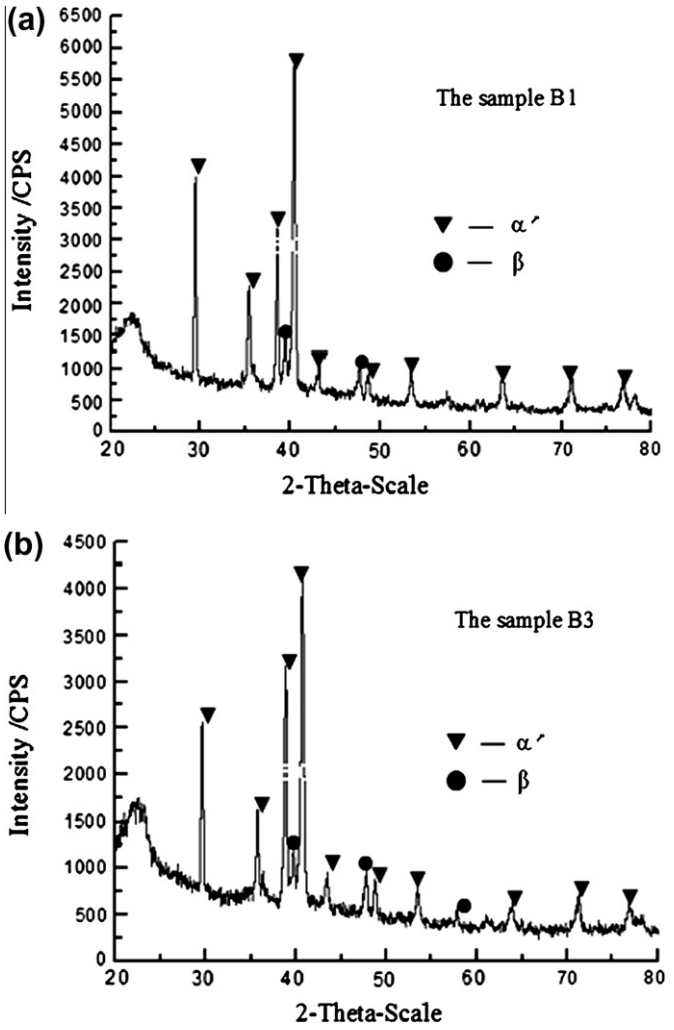

Fig. 4. XRD patterns of Ti–6Al–4V EBW joints: (a) joint B1 and (b) joint B3.

phase transforms to high-temperature β phase simultaneously or successively, and this diffusional transformation precedes the martensitic reaction that occurs subsequently [16]. The transformation of high-temperature β to α′ phase is conducted by means of diffusion or shear, or both of them during the cooling process. When the temperature decreases to the coexisting state of solid phase and liquid phase, primary α′ phase nucleates by attaching to the surface of grains nearby fusion zone and grows toward the center of weld metal to form columnar crystals [20]. The columnar crystals go through β grains and divide them, presenting parallel lath-shaped and epitaxial solidification. The secondary α′ phases of various sizes and crystallographic orientations form in some regions separated by primary α′ phase, as shown in Fig. 5b. When the transformation process is completed, the primary α′ and primary α′, or the primary α′ and secondary α′ contact with each other, which results in acicular or basket-weave pattern microstructure. During welding, with the relatively short holding time of high temperature and higher cooling rate of melting materials, the fine grains will be obtained. Such fine grains contribute directly to the tensile strength of welded joints, as can be seen in mechanical properties tests in the following.

Fig. 6 is another micrograph of weld metal in joint B3. The right side image is the amplified one of local weldment, corresponding to rectangular region in the left side image. From Fig. 6, it can be seen that there are lots of small regions of fixed orientation acicular α′, varying in size, where they separately distribute with clear borders. The needle-like microstructure has a strong tendency to the same orientation in every region, and different regions appear randomly in all directions. In every region, many crystal nucleus may generate simultaneously, and these crystal nucleus are affected by the same weld thermal cycle and begin to grow along the same orientation, while the surrounding ones experience different courses and are limited to extend by one another.

Fig. 7 shows a significant difference between the width of joints B1 and B3 (B2 is almost the same as B1, and B4 as B3). The weldment width of joint B1 is about 3800 μm, much less than 6000 μm of joint B3. Because the heat inputs for B1 and B3 are 180 J/mm and 432 J/mm respectively (referred to Table 2, and the thermal efficiency coefficient is 0.9), the width of weldment depends directly on the heat input. With the prerequisite of full penetration of plates, the molten material will solidify owing to such rapid welding speed of 900 mm/min (B1) or 600 mm/min (B2) before the gap is fully filled with weld metal. As a result, the width is very short (Fig. 7a) and the appearance of weld continuously rises and falls. At the lower welding speed of 300 mm/min, higher heat gets from the melted material, therefore the weldments B3 and B4 are wider than that of B1 and B2. It is also found that narrower weldments do not directly contribute to the joints but reduce the tensile strength of joints. In fact, the wider weldment results in high tensile strength of joints. These phenomena may attribute to the combined effects of welding parameters rather than any single factor such as heat input.

During welding, the structural transformation of HAZ is important to the mechanical properties of welded joints, so it is of much concern. According to Ref. [21], when processed below the transus, Ti–6Al–4V alloy shows an (α + β) structure with the prior α phase retained to room temperature and the β phase transformed in part. As described above, the base metal has colony type of microstructure, and parallel strips α phase is separated by β phase, while the weld metal is almost full of α′ martensite phase. Compared with the weld metal, the maximum temperature of HAZ is lower and there is little change of alloying elements, thus the cooling rate is the critical factor to the structural transformation [22]. Ahmed and Rack have investigated the effects of cooling rate from elevated temperature on phase transformations in α + β titanium alloys during thermal processing [23]. Obviously, the cooling rate of HAZ is faster than that of weld metal, and only a small quantity of acicular α′ phase dissolves from the solidified β phase. The transformation of β to α′ has not taken place completely. Meanwhile, there is not enough heat input and time for initial α and β phases to transform into high-temperature β phase [24], while parts of β still remain in original base metal, and the transformation from β to α′ martensite phase has not been fully completed either. Consequently, the HAZ shows a mixed mode of transformation, which consists of an initial diffusional transformation and a subsequent martensitic transformation [16].

3.2. Mechanical properties

3.2.1. Microhardness

The microhardness of the weld metal, HAZ and base metal are tested and the distribution curves are given in Fig. 8. It displays that the hardness is marginally higher in the weld metal compared with the HAZ and base metal. Lu et al. also reported that the microhardness values for weld zone are higher than that of base metal [24]. The mean value of hardness increases in the weld metal of joints B1 and B2 by about 58 HV, in HAZ by about 32 HV as against the hardness of 355 HV in base metal. The hardness of joints B1 and B2 are higher than that of joints B3 and B4. The first reason is that there are the compact regions of α′ with high density dislocations and phase boundaries in joints B1 and B2, and the second reason is that the microstructures are different as discussed above.

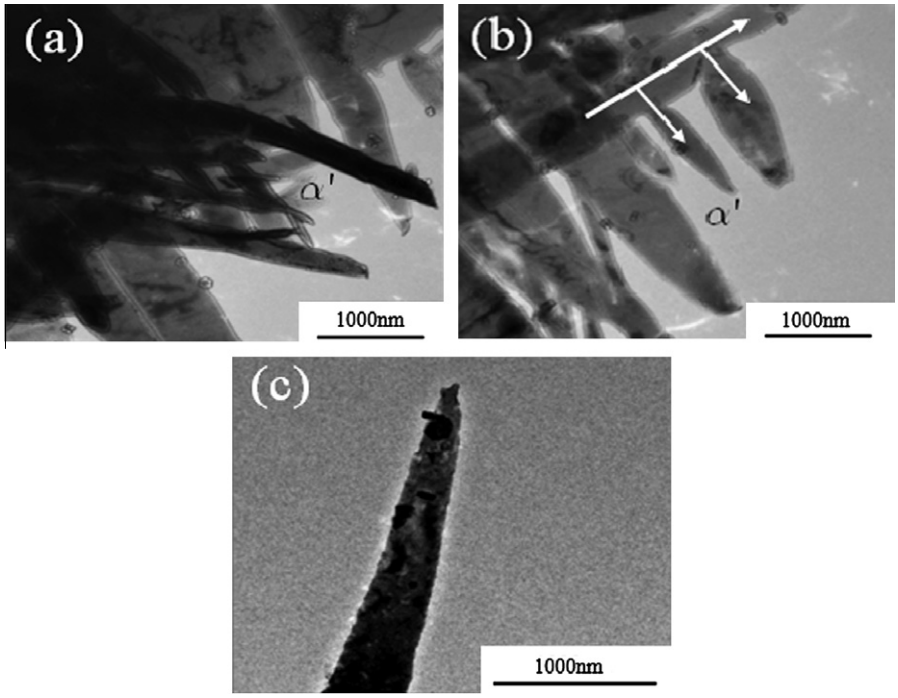

Fig. 5. TEM micrographs of Ti–6Al–4V joints: (a) secondary acicular α′, (b) growing direction of α′ and (c) single acicular α′.

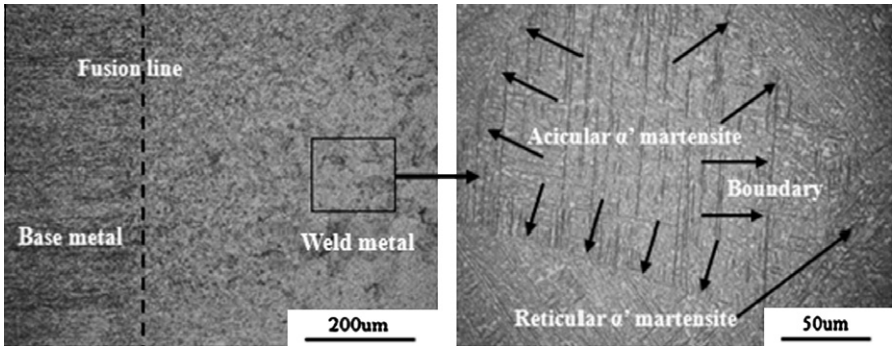

Fig. 6. Regions of α′ martensitic phase in weld metal.

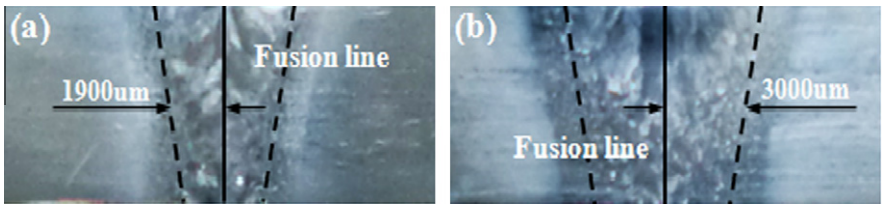

Fig. 7. Width of Ti–6Al–4V EBW joints: (a) joint B1 and (b) joint B3.

Usually, the hardness of β phase is lower than that of α phase, which can be considered as a hard phase in Ti–6Al–4V alloy base metal. The hardness of α′ is just a little higher than that of α-based solid solution, thus it contributes a little to alloy strengthening. However, it is important that there mainly are α′ phase in the weld metal compared with the base metal of α + β duplex phases. Because of the formation of α′ martensitic phase and no more α phase in the weldment [25], the hardness of welded joints increases obviously.

3.2.2. Tensile strength and fractography

Results of tensile test are given in Table 3. It indicates that the joints have different tensile strength with respect to different welding parameters. For comparison, tensile strength of base metal is also listed in Table 3. The fracture positions of welded joints locate respectively in FZ (B1), HAZ (B2), BM (B3 and B4), and the tensile strength of joints is 857.3 MPa, 892.4 MPa, 930.2 MPa and 920.6 MPa respectively. According to the evaluation standard of tensile test, if the tensile strength of joint is higher than the

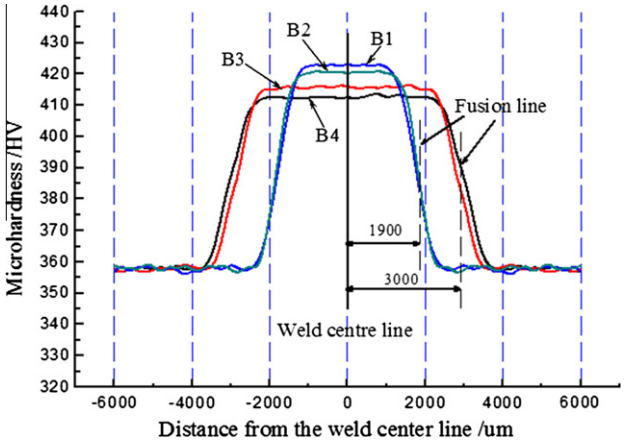

Fig. 8. Microhardness of different Ti–6Al–4V weld metals.

minimum strength of base metal under the condition of practical application, the joints B1 and B2 are still qualified even though fractured in FZ or HAZ. The tensile strength of joints B3 and B4 are higher, which nearly equals to the tensile strength of base metal, and they fracture in base metal far from the weldment, which can meet the requirement of mechanical performance in most cases.

Table 3
Tensile strength of welded joints and base metal.

No.	Tensile strength σ_b (MPa)	Elongation δ (%)	Fracture position
Base metal	932.4	13.1	BM
B1	857.3	9.0	FZ
B2	892.4	10.7	HAZ
B3	930.2	12.8	BM
B4	920.6	11.9	BM

Note: BM – Base Metal; FZ – Fusion Zone; HAZ – Heat-affected Zone.

From Table 3, it also can be seen that the plasticity of base metal are better than that of weld metal and HAZ. According to its microstructure presented above, coarser microstructure will result in low tensile strength while fine and intermediate microstructures have high tensile strength. Results show that under the action of tensile stress, the crack in the joint mainly results from the coarse grain of material, and it is well in accordance with the relationship between the microstructure and mechanical properties of joints.

The different fracture positions suggest that there exist various fracture morphologies in weld metal, HAZ and base metal. To understand it better, SEM images of joints fracture are given in Fig. 9. There are lots of dimples with different size and depth in

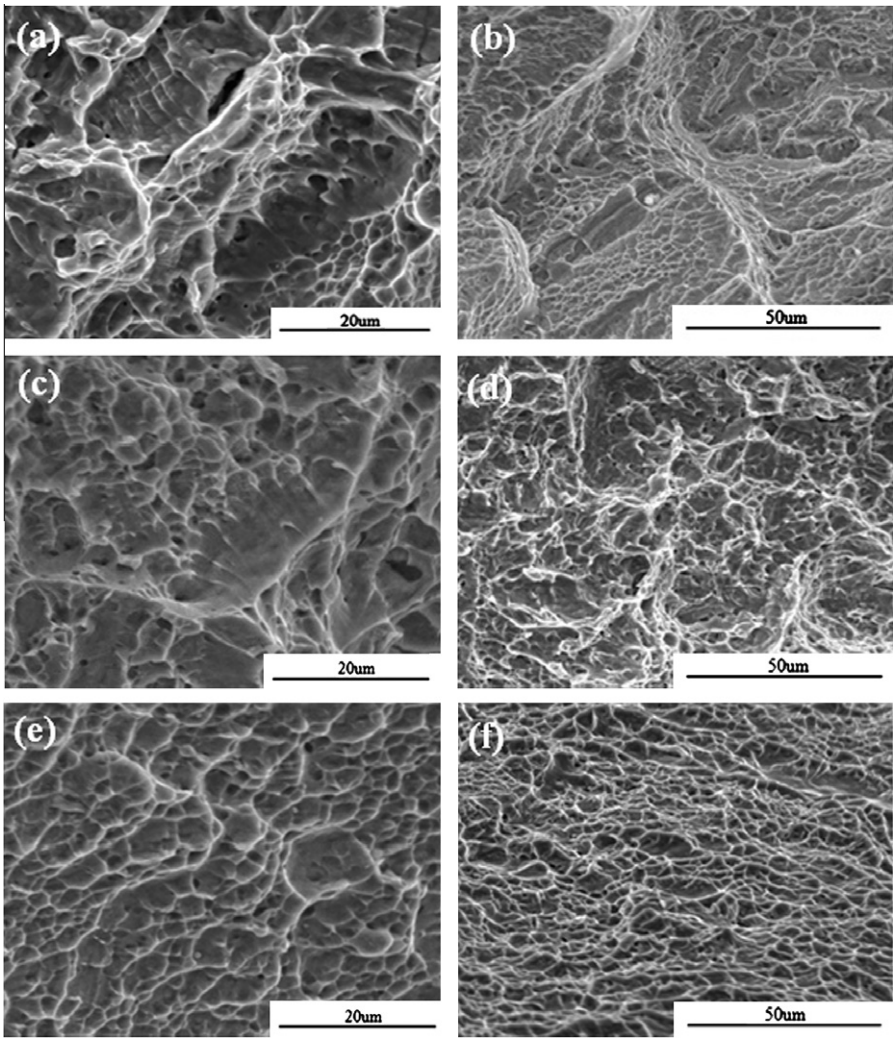

Fig. 9. SEM micrographs of Ti–6Al–4V joint fracture: (a) high amplification of joint B1, (b) low amplification of joint B1, (c) high amplification of joint B2, (d) low amplification of joint B2, (e) high amplification of joint B3 and (f) low amplification of joint B3.

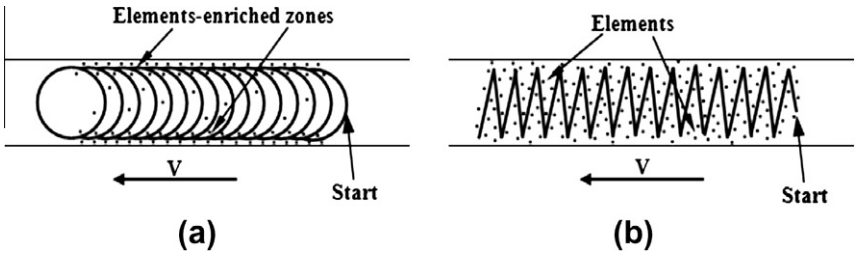

Fig. 10. Elements distribution for different beam scanning patterns: (a) circular scanning and (b) linear scanning.

the fracture surfaces of joints B1 and B2, and obvious tear ridges as well. The fracture surface presents typically the characteristic of ductile. Some dimples of joint B1 are deep and accumulate in strips, while others are shallow and are separated by strips. The dimples in or out of strips is of different size. Some are equiaxed and some have a great deal of tear ridges, as shown in Fig. 9a and b.

As for the fracture morphologies of joint B2, some dimples are equiaxed and some have abundant tear ridges, and some are closely arranged, as shown in Fig. 9c and d. Microcracks form and diffuse firstly in the slip planes as subjected to the action of high tensile stress, and large amounts of dislocation happens instantly in front of the microcracks. In addition, some stress will be released in the course, promoting the formation of secondary microcracks, which distribute in varied parallel levels from primary ones. With the effect of laceration, fracture morphologies of joints in Fig. 9a–d generate respectively.

Fracture morphologies of joint B3 are shown in Fig. 9e and f, which is fractured in the base metal. From the micrographs, almost all equiaxed dimples uniformly distribute in the whole fracture surface with a few tear ridges. The fracture surface presents typical characters of toughness like that of joints B1 and B2. However, the shape of dimples is of much difference, and the microcracks propagation path as well as tensile failure energy is also different. Such dimples are shown in Fig. 9e and f, which lead to high toughness compared with the former.

3.3. The effect of electron beam scanning

Generally, the occurrence of titanium alloy elements segregation in the weldment at the rapid cooling rate is inevitable [26], especially β stabilized elements such as vanadium or iron. At such a cooling rate of weld metal, the grain boundaries will become the solute-riched regions accompanied by the grains growing. The structure of weldment may present columnar crystals with oppositifolious character while cooling. It is similar to the electron beam welds of near-α titanium alloy comprised of columnar grain structure, as described in Ref. [5]. The formation of columnar crystals readily makes solute segregation in grains boundaries, which has great help to epitaxial growth but is at the expense of heterogeneous nucleation in molten pool. As a result, it will bring unfavorable effects to the grain fining. Results show that cracking on joint in the course of tensile mainly results from the coarser grain of material. In addition, the growth of columnar crystals can cause grooves in grain boundaries and supply space for solute atoms accumulation. In order to obtain the welded joint where alloy elements distribute uniformly in weld metal, the electron beam scanning is employed during welding to identify appropriate condition for the electron beam to stir periodically the solute atoms segregated in front of the solid–liquid interface, to improve the mechanical performance of weldment caused by segregation.

Fig 3 shows that the beam scanning used in welding does not necessarily fine the grain and improve the microstructure, and it depends on scanning patterns. The circular beam scanning weakens instead of fining the microstructure, and the acicular phase is coarser than without beam scanning as shown in Fig. 3a. The reason may refer to some elements' heterogeneous distribution affected by circular scanning. In the course of circular scanning, the first circles are basically overlapped by ones that come next, and two lines are formed along the edge of weld, as shown in Fig. 10a. Alloy elements tend to concentrate inevitably in the region of periodic vibration, and segregation of β stabilized elements is not improved effectively. Circular beam scanning stirs the molten pool but does not serve as a useful means in fining grains.

Linear scanning pattern has great effect in fining grain as illustrated in Fig. 3b and c. The moving path of electron beam is in the single direction, and the lines do not connect with or overlap one another, and the distance between lines is the same. The lines have hardly any influence on the preceding ones. The extent of element's macro-segregation is reduced and micro-segregation of β stabilized elements is greatly controlled. The alloy elements uniformly distribute in the melted metal, as shown in Fig. 10b. Meanwhile, the linear scanning pattern can break the big acicular α′ martensitic phase which is possibly growing, and interrupt the single direction of grains which are growing and promote more nucleus formation. As a result, the microstructure is full of fine acicular or cross-cross martensitic phase.

4. Conclusions

Ti–6Al–4V alloys were welded by electron beam welding with different scanning patterns and welding parameters. Based on the experimental results and discussion, some conclusions are drawn as follows.

The weld metal is full of cross-cross acicular α′ martensitic structure while the base metal is of the equiaxed structure. XRD analysis indicates that the FZ mainly consists of α′ martensitic phase and of a small quantity of β phase. The mono-phase martensitic structure greatly contributes to the mechanical properties of welded joints.

The tensile strength of weld metals nearly equals to that of base metal, and fracture occurs in base metal far from weldment with the optimized parameters. Microhardness of weld metals is higher than that of the base metal counterpart due to the formation of α′ martensitic phase. It is well in accordance with the relationship between the microstructure and mechanical properties.

The fracture characterization and positions of electron beam welded joints show the different fracture morphologies. The tensile fracture of base metal and joints present the ductile fracture pattern, which is related to bigger and deeper dimples with mean size in base metal while the dimples are small and shallow with different sizes in weldment or HAZ.

The use of scanning in electron beam welding does not necessarily improve the performance of joints, however, the pattern of linear scanning plays an active role during welding while the circular scanning does not. The microstructure is coarser when circular

scanning is employed, while it is finer with linear scanning, and the mechanical properties of welded joint with circular scanning decrease to a certain extent.

References

[1] Boyer RR. An overview on the use of titanium in the aerospace industry. Mater Sci Eng A 1996;213:103–14.
[2] Picu RC, Majorell A. Mechanical behavior of Ti–6Al–4V at high and moderate temperatures – Part II: Constitutive modeling. Mater Sci Eng A 2002;326:306–16.
[3] Barreda JL, Santamaría F, Azpiroz X, Irisarri AM, Varona JM. Electron beam welded high thickness Ti6Al4V plates using filler metal of similar and different composition to the base plate. Vacuum 2001;62:143–50.
[4] Saresh N, Pillai M Gopalakrishna, Jose Mathew. Investigations into the effects of electron beam welding on thick Ti–6Al–4V titanium alloy. J Mater Process Technol 2007;192–193:83–8.
[5] Meshram Suresh D, Mohandas T. A comparative evaluation of friction and electron beam welds of near-α titanium alloy. Mater Des 2010;31:45–52.
[6] Wanjara P, Brochu M, Jahazi M. Ti–6Al–4V electron beam weld qualification using laser canning confocal microscopy. Mater Charact 2005;54:254–62.
[7] Karimzadeh F, Heidarbeigy M, Saatchi A. Effect of heat treatment on corrosion behavior of Ti–6Al–4V alloy weldments. J Mater Process Technol 2008;206:388–94.
[8] Prasad Rao K, Angamuthu K, Bala Srinivasan P. Fracture toughness of electron beam welded Ti6Al4V. J Mater Process Technol 2008;199:185–92.
[9] Irisarri AM, Barreda JL, Azpiroz X. Influence of the filler metal on the properties of Ti–6Al–4V electron beam weldments. Part I: Welding procedures and microstructural characterization. Vacuum 2010;84:393–9.
[10] Yung Winco KC, Ralph B, Lee WB, Fenn R. An investigation into welding parameters affecting the tensile properties of titanium welds. J Mater Process Technol 1997;63:759–64.
[11] Casavola C, Pappalettere C, Pluvinage G. Fatigue resistance of titanium laser and hybrid welded joints. Mater Des 2011;32:27–35.
[12] Casalino G, Curcio F, Memola Capece Minutolo F. Investigation on Ti6Al4V laser welding using statistical and Taguchi approaches. J Mater Process Technol 2005;167:422–8.
[13] Sun Z, Karppi R. The application of electron beam welding for the joining of dissimilar metals: an overview. J Mater Process Technol 1996;59:257–67.
[14] Jonghyun Kim, Kawamura Y. Electron beam welding of the dissimilar Zr-based bulk metallic glass and Ti metal. Scripta Mater 2007;56:709–12.
[15] Mohandas T, Banerjee D, Kutumba Rao VV. Observations on impact toughness of electron beam welds of an α + β titanium alloy. Mater Sci Eng A 1998;254:147–54.
[16] Kishore Babu N, Ganesh Sundara Raman S, Srinivasa Murthy CV, Madhusudhan Reddy G. Effect of beam oscillation on fatigue life of Ti–6Al–4V electron beam weldments. Mater Sci Eng A 2007;471:113–9.
[17] Wang SG, Ji XH, Zhao XQ, Dong NN. Interfacial characteristics of electron beam welding joints of SiCp/Al composites. Mater Sci Technol 2011;27:60–4.
[18] Barreda JL, Azpiroz X, Irisarri AM. Influence of the filler metal on the mechanical properties of Ti–6Al–4V electron beam weldments. Vacuum 2010;85:10–5.
[19] Kobryn PA, Semiatin SL. Microstructure and texture evolution during solidification processing of Ti–6Al–4V. J Mater Process Technol 2003;135:330–9.
[20] Wu W, Cheng GF, Gao HM, Wu L. Microstructure transformation and mechanical properties of TC4 alloy joints welded by TIG. Trans China Weld Inst 2009;30:81–4.
[21] Ding R, Guo ZX, Wilson A. Microstructural evolution of a Ti–6Al–4V alloy during thermomechanical processing. Mater Sci Eng A 2002;327:233–45.
[22] Akman E, Demir A, Canel T, Sinmazçelik T. Laser welding of Ti6Al4V titanium alloys. J Mater Process Technol 2009;209:3705–13.
[23] Ahmed T, Rack HJ. Phase transformations during cooling in α + β titanium alloys. Mater Sci Eng A 1998;243:206–11.
[24] Lu W, Shi YW, Lei YP, Li XY. Effect of electron beam welding on the microstructures and mechanical properties of thick TC4-DT alloy. Mater Des 2012;34:9–15.
[25] Jha Abhay K, Diwakar V, Pant Bhanu, Sreekumar K. Failure analysis of a Ti–6Al–4V gas bottle. Eng Fail Anal 2006;13:843–56.
[26] Han Z, Zhao H, Chen XF, Lin HC. Corrosion behavior of Ti–6Al–4V alloy welded by scanning electron beam. Mater Sci Eng A 2000;277:38–45.